Smart Structures and Systems, *Vol. 15, No. 3 (2015) 847-862*
DOI: http://dx.doi.org/10.12989/sss.2015.15.3.847

Efficient optimal design of passive structural control applied to isolator design

Mahmoud Kamalzare[1a], Erik A. Johnson[*1] and Steven F. Wojtkiewicz[2b]

[1]*Sonny Astani Department of Civil and Environmental Engineering, University of Southern California, 3620 S Vermont Ave, KAP 210, Los Angeles, CA 90089, USA*
[2]*Department of Civil and Environmental Engineering, Box 5710, Clarkson University, Potsdam, NY 13699-5710, USA*

(Received December 18, 2014, Revised January 20, 2015, Accepted January 27, 2015)

Abstract. Typical base isolated buildings are designed so that the superstructure remains elastic in design-level earthquakes, though the isolation layer is often quite nonlinear using, e.g., hysteretic elements such as lead-rubber bearings and friction pendulum bearings. Similarly, other well-performing structural control systems keep the structure within the linear range except during the most extreme of excitations. Design optimization of these isolators or other structural control systems requires computationally-expensive response simulations of the (mostly or fully) linear structural system with the nonlinear structural control devices. Standard nonlinear structural analysis algorithms ignore the localized nature of these nonlinearities when computing responses. This paper proposes an approach for the computationally-efficient optimal design of passive isolators by extending a methodology previously developed by the authors for accelerating the response calculation of mostly linear systems with local features (linear or nonlinear, deterministic or random). The methodology is explained and applied to a numerical example of a base isolated building with a hysteretic isolation layer. The computational efficiency of the proposed approach is shown to be significant for this simple problem, and is expected to be even more dramatic for more complex systems.

Keywords: computationally-efficient simulation; passive structural control; optimal design; lead-rubber bearings.

1. Introduction

Passive structural control strategies (Housner *et al.* 1997, Soong and Dargush 1997) — such as passive (linear or nonlinear) dampers, friction elements, yielding metal elements, isolation devices, and tuned-mass dampers — are some of the most commonly implemented forms of structural control. For linear structures with linear structural control elements, the simulation, design and optimization of such systems is relatively straightforward as linear response computation, driven by deterministic or stochastic excitation, is well-understood and can be performed with good efficiency. However, if the passive control element is nonlinear, or if there are nonlinearities in the structural system model, then the response computation, and any design optimization using the

*Corresponding author, Professor & Associate Chair, E-mail: JohnsonE@usc.edu
[a] Formerly, Graduate Research Assistant, E-mail: kamalzar@usc.edu
[b] Associate Professor, E-mail: swojtkie@clarkson.edu

http://www.techno-press.org/?journal=sss&subpage=8 ISSN: 1738-1584 (Print), 1738-1991 (Online)

responses, becomes more computationally challenging. The typical approach simulates these systems by employing a generic nonlinear solver, a general tool that can be used to simulate a wide variety of dynamical systems, but cannot exploit the localized nature of the passive control elements within the overall model.

This paper proposes a design optimization approach for linear structures with local passive structural control elements, enabled by a computationally-efficient simulation of the structural responses as well as their sensitivities to isolator design parameters. The authors' simulation methodology (Gaurav *et al.* 2011) can be considered an exact model reduction of a linear structure with local features, features that are linear or nonlinear, deterministic or random, to a low-order Volterra integral equation (VIE) in the forces generated by these features. When the number of local features is small relative to the system order, and the local forces depend on a low-rank subset of the system degrees of freedom, this VIE can be solved forward in time with significant reductions in computational requirements relative to those of a conventional nonlinear solver (Kamalzare *et al.* 2015). Further, the authors have shown (Wojtkiewicz and Johnson 2014, Johnson and Wojtkiewicz 2014) how response sensitivities, both gradients and Hessians, can be computed in a similar manner. This paper, then, proposes and implements this methodology for design optimization of passive structural control elements in a realistic structure.

While the approach proposed herein is general, the numerical example is an optimal parameter design of a hysteretic lead-rubber bearing in a base-isolated building. Base isolation (Kelly, 1986; Buckle and Mayes 1990, Skinner *et al.* 1993, Naeim and Kelly 1999) seeks to separate the superstructure from ground motion, insulating it, insofar as is possible, from the excitation. However, there are distinct trade offs between the displacement across the isolation layer and the motion of (and within) the superstructure. The numerical example considered herein is not intended to be an exhaustive study of the optimal isolation problem, but a demonstration of the computational advantages of the proposed simulation methodology for design optimization problems. One of the earliest studies of optimal base isolation parameters is by Bhatti *et al.* (1978). A series of papers by Constantinou and Tadjbakhsh (1983, 1984, 1985) examined optimal isolators with linear stiffness and damping alone (using a frequency domain analysis), and with friction and with hysteretic elements (using linearization), respectively. Park and Otsuka (1999) performed a parameter study, over a (small) grid of values for each key isolator parameter, of the responses of a bridge to scaled versions of the 1940 El Centro earthquake. Jangid studied linearization (Jangid 2000) and time-domain approaches (Jangid 2005, 2007) to find optimal isolation parameters, primarily the isolator yield force, for different isolator types/models. Fragiacomo *et al.* (2003) used energy measures to search for optimal isolator parameters. Others have used probabilistic / reliability approaches, such as Taflanidis and Beck (2008a, b, 2009, 2010), Bucher (2009), Jensen and Sepulveda (2012), and Roy *et al.* (2014).

The nonlinear nature of these systems makes computationally challenging the use of a complex superstructure model to perform a full parameter study or optimization without simplifications. Thus, most studies of optimal isolation design make simplifying assumptions, such as using statistical linearization of the nonlinear hysteresis, or using very simplified models of the superstructure, such as rigid or single-degree-of-freedom (SDOF) models. Conventional model reduction must necessarily make assumptions on the behavior of the nominal system without regard for whether the added localized nonlinearities may excite dynamics that are poorly approximated by the reduced model. Other approximate methods have been employed to study systems with local nonlinearities, including Guyan and static reduction, component mode synthesis, and dynamic condensation; the reader is referred to Gaurav *et al.* (2011), and the

references cited therein, for more details. Another class of approaches, including the fast nonlinear analysis method (Wilson 1999) and the work of Gordis and students (Gordis and Radwick 1999, Norton 2002), computes the response of the locally nonlinear system as the superposition of the response of a related linear system with the addition of a pseudo-force imparted on the nominal linear system by the local features; the authors' analysis method used herein (Gaurav *et al.* 2011) falls in this class as well but, unlike other methods in this class, fully exploits the locality of the nonlinear features and performs an exact model reduction.

The following sections first summarize the proposed formulation for exploiting the localized nature of the nonlinearities to rapidly perform design optimization. Then, a numerical example of an 11-story 2-bay superstructure on an isolation layer demonstrates the efficacy and computational advantages of the proposed method. A lead-rubber isolation bearing is modeled as a Bouc-Wen hysteresis in which the yield force, the pre-yield stiffness and the post-yield stiffness are optimized. The responses and their gradients to the three design variables are used to minimize a mean-square measure of the base drift and roof acceleration subject to physically-meaningful constraints. Finally, a robustness analysis of the optimal design to the sharpness of the hysteresis is conducted.

2. Methodology

The proposed approach is given in this section. First, the computationally-efficient simulation of responses is summarized for linear systems with localized features, using a trapezoidal integration of the convolution integrals to arrive at a VIE (Gaurav *et al.* 2011). Then, the derivation of the sensitivities of these responses to design parameters is summarized (Wojtkiewicz and Johnson 2014). Finally, an extension to a design optimization framework, a preliminary version of which the authors proposed in Johnson *et al.* (2013), is detailed.

2.1 Response calculation

Consider two state-space structural models: a nominal one that is linear in states $\mathbf{x}$, and a related model that is nonlinear in states $\mathbf{X}$, but with the same initial condition $\mathbf{x}_0$ and excitation $\mathbf{w}$

$$\begin{aligned} \dot{\mathbf{x}} &= \mathbf{A}\mathbf{x} + \mathbf{B}\mathbf{w} \\ \dot{\mathbf{X}} &= \mathbf{A}\mathbf{X} + \mathbf{B}\mathbf{w} + \mathbf{L}\mathbf{g}(\mathbf{G}\mathbf{X};\boldsymbol{\theta}) \end{aligned} \qquad \mathbf{X}(0) = \mathbf{x}(0) = \mathbf{x}_0 \tag{1}$$

where $\mathbf{x}$ and $\mathbf{X}$ are each n-element state vectors with state matrix $\mathbf{A}$ and excitation influence matrix $\mathbf{B}$, $\mathbf{g}(\mathbf{G}\mathbf{X};\boldsymbol{\theta})$ is a linear or nonlinear local feature vector function of a subset (or linear combination) $\overline{\mathbf{X}} = \mathbf{G}\mathbf{X}$ of the states and of design parameters $\boldsymbol{\theta}$ (time-invariant, though possibly random), with influence matrix $\mathbf{L}$. While the method is general, it is most efficient when both $\mathbf{G}$ and $\mathbf{L}$ have low rank; *i.e.*, only a few states enter into the nonlinearities, and there are a few local features.

If $\mathbf{p}(t) = \mathbf{g}(\overline{\mathbf{X}}(t);\boldsymbol{\theta})$ were known *a priori*, the principle of superposition dictates that the states $\mathbf{X}(t)$ and responses $\overline{\mathbf{X}}(t)$ of the nonlinear system can be written as the corresponding linear system responses $\mathbf{x}(t)$ and $\overline{\mathbf{x}}(t) = \mathbf{G}\mathbf{x}(t)$ plus convolution integrals involving $\mathbf{p}(t)$

$$\begin{aligned} \mathbf{X}(t) &= \mathbf{x}(t) + \int_0^t \mathbf{H}_{\mathbf{L}}(t-\tau)\mathbf{p}(\tau)\mathrm{d}\tau \\ \overline{\mathbf{X}}(t) &= \overline{\mathbf{x}}(t) + \int_0^t \overline{\mathbf{H}}_{\mathbf{L}}(t-\tau)\mathbf{p}(\tau)\mathrm{d}\tau \end{aligned} \tag{2}$$

where $\mathbf{H}_{\mathbf{L}}(t) = e^{\mathbf{A}t}\mathbf{L}$ is the state response to an impulse in the pattern of $\mathbf{L}$, and $\overline{\mathbf{H}}_{\mathbf{L}}(t) = \mathbf{G}\mathbf{H}_{\mathbf{L}}(t) = \mathbf{G}e^{\mathbf{A}t}\mathbf{L}$. The definition of $\mathbf{p}(t)$ then can be rewritten using Eq. (2)

$$\mathbf{p}(t) - \mathbf{g}\left(\overline{\mathbf{x}}(t) + \int_0^t \overline{\mathbf{H}}_{\mathbf{L}}(t-\tau)\mathbf{p}(\tau)\mathrm{d}\tau;\, \boldsymbol{\theta}\right) = \mathbf{0} \tag{3}$$

which is a system of Volterra integral equations (VIEs) in non-standard form. The authors previously showed (Gaurav *et al.*, 2011) how to solve a time-discretized Eq. (3) using second-order (trapezoidal) or fourth-order quadratures; the former is used herein as follows. Let subscript k denote a quantity at time $t_k = k\Delta t$; thus, $\mathbf{p}_k = \mathbf{p}(t_k)$, $\overline{\mathbf{x}}_k = \overline{\mathbf{x}}(t_k)$, $\overline{\mathbf{X}}_k = \overline{\mathbf{X}}(t_k)$ and $\overline{\mathbf{H}}_{\mathbf{L},k} = \overline{\mathbf{H}}_{\mathbf{L}}(t_k)$. Then, discretize the convolution, separating the portion known prior to time k

$$\overline{\mathbf{X}}_k \cong \boldsymbol{\alpha}_{k-1} + \tfrac{1}{2}\overline{\mathbf{H}}_{\mathbf{L},0}\mathbf{p}_k\Delta t \qquad \text{where} \quad \boldsymbol{\alpha}_{k-1} = \overline{\mathbf{x}}_k + \tfrac{1}{2}\overline{\mathbf{H}}_{\mathbf{L},k}\mathbf{p}_0\Delta t + \sum_{j=1}^{k-1}\overline{\mathbf{H}}_{\mathbf{L},k-j}\mathbf{p}_j\Delta t \tag{4}$$

Substituting the expression for $\overline{\mathbf{X}}_k$ in Eq. (4) back into a time-discretization of the VIE in Eq. (3), and using Newton's method to solve the resulting equation for $\mathbf{p}_k$, gives

$$\mathbf{p}_k^{j+1} = \mathbf{p}_k^{j} - \left[\mathbf{I} - \tfrac{1}{2}\left.\frac{\partial \mathbf{g}}{\partial \overline{\mathbf{X}}}\right|_{\overline{\mathbf{X}}_k,\boldsymbol{\theta}} \overline{\mathbf{H}}_{\mathbf{L},0}\Delta t\right]^{-1}\left[\mathbf{p}_k^{j} - \mathbf{g}\left(\boldsymbol{\alpha}_{k-1} + \tfrac{1}{2}\overline{\mathbf{H}}_{\mathbf{L},0}\mathbf{p}_k^{j}\Delta t;\boldsymbol{\theta}\right)\right] \tag{5}$$

where $\mathbf{p}_k^j$ denotes the j^{th} iteration on the value of $\mathbf{p}_k$, and the initial estimate $\mathbf{p}_k^0 = \mathbf{p}_{k-1}$ is the same as the previous time step. The iteration is terminated once the accuracy requirements are achieved (typical 2–3 iterations are sufficient). (Note: if $\overline{\mathbf{H}}_{\mathbf{L},0}$ were zero, which is the case for most structural systems when $\overline{\mathbf{X}}$ contains only displacements, then no iteration is required at all.) Once the sequence $\{\mathbf{p}_0, \mathbf{p}_1, \ldots\}$ has been determined, the time-discretized states $\mathbf{X}_k$ can be determined from convolution Eq. (2) using any standard approach (e.g., quadratures, FFT, etc.).

2.2 Sensitivity of responses

The sensitivity of $\mathbf{p}(t)$ to some parameter θ_i in $\mathbf{g}(\overline{\mathbf{X}};\boldsymbol{\theta})$ is given by

$$\mathbf{s}^i(t) = \frac{\partial \mathbf{p}(t)}{\partial \theta_i} = \frac{\partial \mathbf{g}}{\partial \theta_i} + \frac{\partial \mathbf{g}}{\partial \overline{\mathbf{X}}}\frac{\partial \overline{\mathbf{X}}}{\partial \theta_i} \tag{6}$$

The modified states depend on $\boldsymbol{\theta}$ only through $\mathbf{p}(t)$ so

$$\frac{\partial \mathbf{X}(t)}{\partial \theta_i} = \int_0^t \mathbf{H}_{\mathbf{L}}(t-\tau)\mathbf{s}^i(\tau)\mathrm{d}\tau \quad \text{and} \quad \frac{\partial \overline{\mathbf{X}}(t)}{\partial \theta_i} = \int_0^t \overline{\mathbf{H}}_{\mathbf{L}}(t-\tau)\mathbf{s}^i(\tau)\mathrm{d}\tau \tag{7}$$

$$\frac{\partial \overline{\mathbf{X}}_k}{\partial \theta_i} \cong \boldsymbol{\kappa}_{k-1} + \tfrac{1}{2}\overline{\mathbf{H}}_{\mathbf{L},0}\mathbf{s}_k^i\Delta t \quad \text{where} \quad \boldsymbol{\kappa}_{k-1} = \tfrac{1}{2}\overline{\mathbf{H}}_{\mathbf{L},k}\mathbf{s}_0^i\Delta t + \sum_{j=1}^{k-1}\overline{\mathbf{H}}_{\mathbf{L},k-j}\mathbf{s}_j^i\Delta t \tag{8}$$

where a trapezoidal integration is used to approximate the convolution. Substituting Eq. (8) into Eq. (6) evaluated at time t_k, and solving for sensitivity $\mathbf{s}_k^i$ gives straightforward matrix solution

$$\mathbf{s}_k^i = [\mathbf{I} - \tfrac{1}{2}\mathbf{E}_k \overline{\mathbf{H}}_{\mathbf{L},0}\Delta t]^{-1}[\mathbf{d}_k + \mathbf{E}_k \boldsymbol{\kappa}_{k-1}] \quad \text{where} \quad \mathbf{d}_k^i = \left.\frac{\partial \mathbf{g}}{\partial \theta_i}\right|_{\overline{\mathbf{X}}_k,\boldsymbol{\theta}} \quad \text{and} \quad \mathbf{E}_k = \left.\frac{\partial \mathbf{g}}{\partial \overline{\mathbf{X}}}\right|_{\overline{\mathbf{X}}_k,\boldsymbol{\theta}} \tag{9}$$

The full state sensitivity $\partial \mathbf{X}_k / \partial \theta_i$ can then be found from convolution Eq. (7) using any conventional method (e.g., quadratures, FFT, etc.). If needed by the optimization, second-order sensitivities (Hessians) can be found with a similar approach (Wojtkiewicz and Johnson 2014).

2.3 Optimization procedure

Consider a design optimization problem with cost functional $J(\widetilde{\mathbf{X}}(t;\boldsymbol{\theta}))$, where $\widetilde{\mathbf{X}} = \widetilde{\mathbf{G}}\mathbf{X}$ is some linear combination of the states, and the "optimal" value of the design parameter(s) $\boldsymbol{\theta}$ is desired. To find the design point where J is minimized, one may employ non-gradient-based or gradient-based approaches. For the former, the proposed approach can be used to efficiently compute the response $\widetilde{\mathbf{X}}(t;\boldsymbol{\theta})$, from which the cost functional J is determined. To implement a gradient-based optimization algorithm, the gradient $\partial J/\partial \boldsymbol{\theta}$ of the cost functional with respect to the design parameters may be approximated by numerical methods such as finite differences, or it can be provided using the response sensitivities in Eq. (9), requiring fewer function evaluations and, thus, more computationally efficient and, typically, more accurate. The cost functional derivatives with respect to the design parameters can be calculated using

$$\frac{\partial J(\widetilde{\mathbf{X}}(t;\boldsymbol{\theta}))}{\partial \boldsymbol{\theta}} = \frac{\partial J(\widetilde{\mathbf{X}}(t;\boldsymbol{\theta}))}{\partial \widetilde{\mathbf{X}}} \frac{\partial \widetilde{\mathbf{X}}}{\partial \boldsymbol{\theta}}, \qquad \frac{\partial \widetilde{\mathbf{X}}}{\partial \theta_i} = \int_0^t \widetilde{\mathbf{G}}\mathbf{H}_{\mathbf{L}}(t-\tau)\mathbf{s}^i(\tau)\mathrm{d}\tau \tag{10}$$

where $\partial \widetilde{\mathbf{X}} / \partial \theta_i$ can be computed using the sensitivities $\mathbf{s}_k^i$ from Eq. (9) in any usual way. (Note that an additional term appears in Eq. (10) if J also has explicit dependence on $\boldsymbol{\theta}$.)

With this computationally-efficient approach for determining the cost functional J and its sensitivities in Eq. (10) to the design variables, a design optimization that requires many function evaluations can be performed in a manner that is much faster than if the response and sensitivity simulation utilizes conventional nonlinear solvers that cannot exploit the localized nature of the isolators or other structural control devices. The primary focus of this study is to propose the use of this VIE approach for design optimization of (nonlinear) passive structural control devices. The numerical example that follows is just one such application of this method.

3. Numerical example: Optimal design of isolation hysteresis for isolated building

This example demonstrates how the proposed method can be utilized for designing an optimal hysteretic isolator in the isolation layer of a 100-degree-of-freedom (DOF) frame structure. In this example, the proposed method calculates both the responses and sensitivities for use in a gradient-based optimization algorithm, which determines the optimal strategy in a very computationally efficient manner.

Consider the base isolated building in Fig. 1(a). The superstructure is 11 stories tall and 2 bays wide; the superstructure is treated as linear, with horizontal, vertical and rotational DOFs at each moment-bearing joint. The superstructure, if it were a fixed-base structure, would have a fundamental period of 1.05 s. As a fixed base structure, the equations of motion would be

$$\mathbf{M}_s\ddot{\mathbf{u}}_s + \mathbf{C}_s\dot{\mathbf{u}}_s + \mathbf{K}_s\mathbf{u}_s = -\mathbf{M}_s\mathbf{r}\ddot{u}_g \tag{11}$$

where $\mathbf{u}_s$ is a vector of generalized displacements of the structure relative to the ground, for a total of 99 DOFs, three at each of the 33 nodes; the superstructure consistent mass and stiffness matrices are denoted $\mathbf{M}_s$ and $\mathbf{K}_s$, respectively; the damping matrix $\mathbf{C}_s$ is computed using the Rayleigh method by assuming that the 1st and 10th modal damping ratios are each 3%; $\ddot{u}_g$ is the horizontal ground acceleration; and $\mathbf{r} = [1\ 0\ 0\ \ 1\ 0\ 0\ \ \ldots\ \ 1\ 0\ 0]^T$ (i.e., a 1 in each element corresponding to a horizontal displacement in $\mathbf{u}_s$, and zeros elsewhere) is the influence vector.

3.1 Hysteretic isolation: A lead-rubber bearing system

The structure sits on a base mass that is supported by an isolation layer composed of lead-rubber bearings (LRBs). The base drift is assumed sufficiently moderate that the low-damping rubber acts as a linear stiffness and viscous damping element. The lead plug is assumed to provide linear stiffness before yielding, and then a much lower (or zero) stiffness thereafter. Together, the rubber and the lead provide a hysteretic stiffness such as shown in Fig. 1b. While a bilinear model is commonly used for LRBs, it has been shown to result in computed accelerations that are larger than those observed (Skinner *et al.* 1993, Nagarajaiah and Sun 2000) as it overstates the sharpness of the lead transition from fully elastic to (partially) plastic; instead here, the computationally more tractable, smooth Bouc-Wen model (Bouc 1967, Wen 1976) is used. (The effect of elastic-to-partially-plastic transition sharpness is discussed in greater detail in §3.8.)

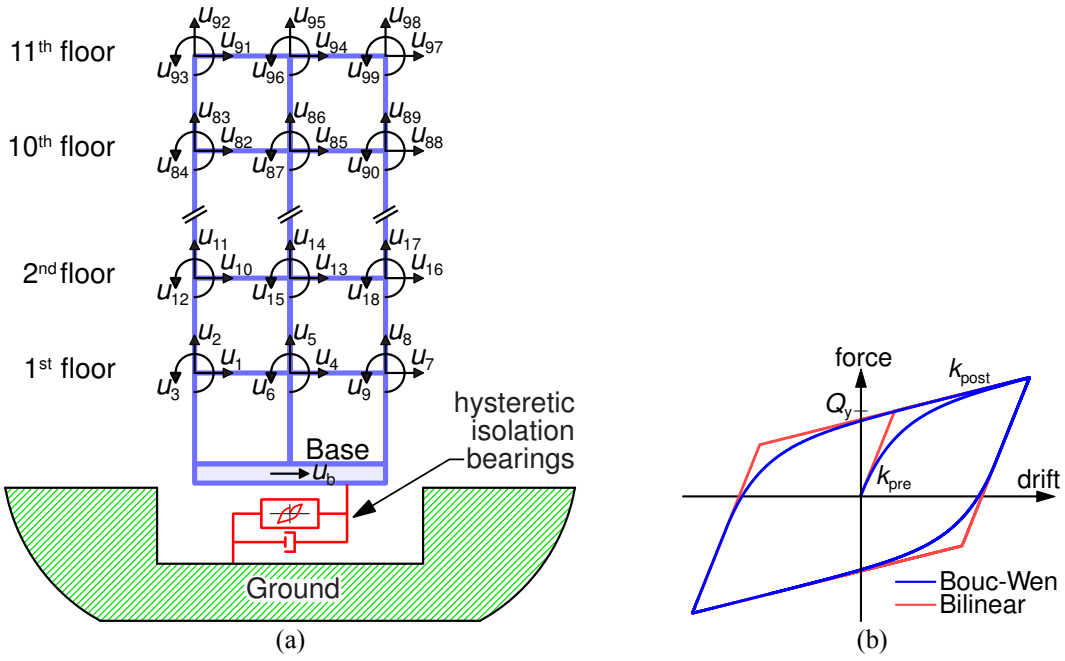

Fig. 1 (a) 100 DOF base-isolated structure and (b) bilinear and Bouc-Wen hysteresis loops

The nominal post-yield stiffness k_{post} and base mass m_b are chosen such that the fundamental mode of the isolated building, if the yield force Q_y were zero, would have a period of 2.76 s, which is in the typical expected range (Skinner *et al.* 1993); k_{pre} is the pre-yield stiffness; the isolation-layer viscous damping coefficient c_b, provided by the isolator (and/or supplemental passive viscous dampers), is chosen such that the isolation mode has a damping ratio of about 5.5%. The building weight (base plus superstructure) is $W = 1.28$ MN and its height from the base upwards is $h = 44$ m. The isolation layer is assumed to be constrained to move in the horizontal direction only, so multiple identical LRBs can be modeled as a single LRB. The result is a 100-DOF isolated structure model. The primary ground excitations used herein are the El Centro (N-S Imperial Valley Irrigation District substation record of the 1940 Imperial Valley earthquake; PGA 0.348 *g*) and Northridge (N-S Sylmar County Hospital parking lot record of the 1994 Northridge earthquake; PGA 0.843 *g*) ground motions sampled at 50 Hz (i.e., $\Delta t = 0.02$ s).

The Bouc-Wen model introduces an evolutionary variable z that is proportional to the base drift u_b for small motion, but asymptotically approaches ±1 for large motion as the lead shears (or a friction pendulum isolator surface slides). The equations of motion of the base mass are given by

$$m_b\ddot{u}_b + c_b\dot{u}_b + k_{post}u_b + \alpha z = -m_b\ddot{u}_g + \mathbf{r}^T\mathbf{C}_s(\dot{\mathbf{u}}_s - \mathbf{r}\dot{u}_b) + \mathbf{r}^T\mathbf{K}_s(\mathbf{u}_s - \mathbf{r}u_b) \tag{12a}$$

$$\dot{z} = A\dot{u}_b - \beta\dot{u}_b|z|^n - \gamma z|\dot{u}_b||z|^{n-1} \tag{12b}$$

where $\alpha = Q_y[1 - (k_{post}/k_{pre})]$ is the peak of the non-elastic force; $A = 2\beta = 2\gamma = k_{pre}/Q_y$ (which constrains $z \in [-1,1]$ and makes identical the loading and unloading stiffnesses); and the exponent n controls the sharpness of the hysteresis loop. The superstructure equations of motion, with displacements $\mathbf{u}_s$ relative to the ground, are given by

$$\mathbf{M}_s\ddot{\mathbf{u}}_s + \mathbf{C}_s(\dot{\mathbf{u}}_s - \mathbf{r}\dot{u}_b) + \mathbf{K}_s(\mathbf{u}_s - \mathbf{r}u_b) = -\mathbf{M}_s\mathbf{r}\ddot{u}_g \tag{13}$$

Combining the equations of motion in Eqs. (12 (a)) and (13) yields

$$\mathbf{M}\ddot{\mathbf{u}} + \mathbf{C}\dot{\mathbf{u}} + \mathbf{K}\mathbf{u} = -\mathbf{M}\tilde{\mathbf{r}}\ddot{u}_g - [1 \quad \mathbf{0}^T]^T[\alpha z + (k_{post} - k_b)u_b]$$

$$\mathbf{M} = \begin{bmatrix} m_b & \mathbf{0}^T \\ \mathbf{0} & \mathbf{M}_s \end{bmatrix}, \quad \mathbf{C} = \begin{bmatrix} c_b + \mathbf{r}^T\mathbf{C}_s\mathbf{r} & -\mathbf{r}^T\mathbf{C}_s \\ -\mathbf{C}_s\mathbf{r} & \mathbf{C}_s \end{bmatrix}, \quad \mathbf{K} = \begin{bmatrix} k_b + \mathbf{r}^T\mathbf{K}_s\mathbf{r} & -\mathbf{r}^T\mathbf{K}_s \\ -\mathbf{K}_s\mathbf{r} & \mathbf{K}_s \end{bmatrix} \tag{14}$$

where $\mathbf{u}(t) = [u_b(t) \quad \mathbf{u}_s^T(t)]^T$ is the generalized displacement vector and $\tilde{\mathbf{r}} = [1 \quad \mathbf{r}^T]^T$. Note that, since $k_{post}u_b + \alpha z$ cannot be in the nominal system in Eq. (12(a)), as it depends on design parameters, $k_b u_b$ is added to both sides of the equation to preserve the stability of the nominal system, where $k_b = 750$ kN/m is the nominal post-yield stiffness that results in the 2.76 s isolation period. The equation of motion in Eq. (14) can be rewritten in the state space form of Eq. (1) with

$$\mathbf{X} = \begin{Bmatrix} \mathbf{u} \\ \dot{\mathbf{u}} \\ z \end{Bmatrix}, \quad \mathbf{A} = \begin{bmatrix} \mathbf{0} & \mathbf{I} & \mathbf{0} \\ -\mathbf{M}^{-1}\mathbf{K} & -\mathbf{M}^{-1}\mathbf{C} & \mathbf{0} \\ \mathbf{0}^T & \mathbf{0}^T & 0 \end{bmatrix}, \quad \mathbf{B} = \begin{Bmatrix} \mathbf{0} \\ -\tilde{\mathbf{r}} \\ 0 \end{Bmatrix}, \quad \mathbf{L} = \begin{bmatrix} \mathbf{0} & \mathbf{0} \\ -\mathbf{M}^{-1}[1 \quad \mathbf{0}^T]^T & \mathbf{0} \\ 0 & 1 \end{bmatrix} \tag{15}$$

and a modification $\mathbf{g}$ that is a 2×1 vector function

$$\mathbf{g}(\overline{\mathbf{X}};\boldsymbol{\theta}) = \begin{Bmatrix} \alpha z + (k_{post} - k_b)u_b \\ A\dot{u}_b - \beta\dot{u}_b|z|^n - \gamma z|\dot{u}_b||z|^{n-1} \end{Bmatrix} \tag{16}$$

where $\overline{\mathbf{X}}(t)=[u_\mathrm{b} \quad \dot{u}_\mathrm{b} \quad z]^\mathrm{T}$ and $\boldsymbol{\theta}=[Q_\mathrm{y} \quad k_\mathrm{pre} \quad k_\mathrm{post}]^\mathrm{T}$. While Q_y and k_pre do not appear explicitly in Eq. (16), α, A, β and γ are functions of them. Since g_1 is linear in the states, it would typically be included in the nominal system (in $\mathbf{A}$); since g_1 depends on $\boldsymbol{\theta}$, it is excluded from the nominal system so that $\boldsymbol{\theta}$ can be varied as a modification to the nominal system. The exponent n is considered initially to be 1, which results in smooth hysteresis loops, but relaxed in §3.8.

3.2 Baseline LRB design

To provide a performance baseline, the same structure equipped with an LRB system, with the suggested (Skinner *et al.* 1993) yield force of 5% of the building weight for small to moderate earthquakes such as El Centro and 15% for strong earthquakes such as Northridge, and pre-yield to post-yield stiffness ratios of 6 and 10 for moderate and strong excitations, respectively (the values most commonly used in the literature). Thus, the two baseline designs are: (a) for El Centro, an LRB with a yield force $0.05W$, pre-yield stiffness $6k_\mathrm{b}$ and post-yield stiffness k_b; i.e., $\boldsymbol{\theta}^0_\mathrm{EC}=[0.05W \quad 6k_\mathrm{b} \quad k_\mathrm{b}]^\mathrm{T}$; and (b) for Northridge, an LRB with a yield force $0.15W$, pre-yield stiffness $10k_\mathrm{b}$ and post-yield stiffness k_b; *i.e.*, $\boldsymbol{\theta}^0_\mathrm{N}=[0.15W \quad 10k_\mathrm{b} \quad k_\mathrm{b}]^\mathrm{T}$. For a baseline LRB system, one may select either a smooth or bilinear hysteresis; the latter (using an $n=100$ Bouc-Wen model as an approximation) is adopted here due to its wide usage in the literature, with root mean square (RMS) base drift and roof acceleration of 1.84 cm and 77.40 cm/s^2, respectively, for El Centro, and 6.34 cm and 130.22 cm/s^2, respectively, for Northridge.

3.3 Sensitivity formulation

For this numerical example, the sensitivity to each design parameter is computed analytically. The required partial derivatives of $\mathbf{g}$ with respect to the parameters $\boldsymbol{\theta}$ and to the states $\overline{\mathbf{X}}$, are

$$\mathbf{d}^1_k=\left.\frac{\partial \mathbf{g}}{\partial \theta_1}\right|_k=\begin{Bmatrix}\partial g_1/\partial Q_\mathrm{y}\\ \partial g_2/\partial Q_\mathrm{y}\end{Bmatrix}_k=\begin{Bmatrix}z[1-(k_\mathrm{post}/k_\mathrm{pre})]\\ [\tfrac{1}{2}\dot{u}_\mathrm{b}|z|^n+\tfrac{1}{2}|\dot{u}_\mathrm{b}||z|^{n-1}-\dot{u}_\mathrm{b}]k_\mathrm{pre}/Q_\mathrm{y}^2\end{Bmatrix}_k \tag{17a}$$

$$\mathbf{d}^2_k=\left.\frac{\partial \mathbf{g}}{\partial \theta_2}\right|_k=\begin{Bmatrix}\partial g_1/\partial k_\mathrm{pre}\\ \partial g_2/\partial k_\mathrm{pre}\end{Bmatrix}_k=\begin{Bmatrix}zQ_\mathrm{y}k_\mathrm{post}/k_\mathrm{pre}^2\\ [\dot{u}_\mathrm{b}-\tfrac{1}{2}\dot{u}_\mathrm{b}|z|^n-\tfrac{1}{2}z|\dot{u}_\mathrm{b}||z|^{n-1}]/Q_\mathrm{y}\end{Bmatrix}_k \tag{17b}$$

$$\mathbf{d}^3_k=\left.\frac{\partial \mathbf{g}}{\partial \theta_3}\right|_k=\begin{Bmatrix}\partial g_1/\partial k_\mathrm{post}\\ \partial g_2/\partial k_\mathrm{post}\end{Bmatrix}_k=\begin{Bmatrix}u_\mathrm{b}-[zQ_\mathrm{y}/k_\mathrm{pre}]\\ 0\end{Bmatrix}_k \tag{17c}$$

$$\mathbf{E}_k=\left.\frac{\partial \mathbf{g}}{\partial \overline{\mathbf{X}}}\right|_k=\begin{bmatrix}\partial g_1/\partial u_\mathrm{b} & \partial g_2/\partial u_\mathrm{b}\\ \partial g_1/\partial \dot{u}_\mathrm{b} & \partial g_2/\partial \dot{u}_\mathrm{b}\\ \partial g_1/\partial z & \partial g_2/\partial z\end{bmatrix}_k^\mathrm{T}=\begin{bmatrix}k_\mathrm{post}-k_\mathrm{b} & 0\\ 0 & A-\beta|z|^n-\gamma z|z|^{n-1}\operatorname{sgn}\dot{u}_\mathrm{b}\\ \alpha & -\beta n\dot{u}_\mathrm{b}|z|^{n-1}\operatorname{sgn} z-\gamma n|\dot{u}_\mathrm{b}||z|^{n-1}\end{bmatrix}_k^\mathrm{T} \tag{18}$$

where the subscript k denotes evaluation at time $k\Delta t$. For example, the sensitivities of the base drift with respect to Q_y, k_pre and k_post (at the design point discussed subsequently) are shown in Fig. 2, along with those obtained by numerical integration of the analytical sensitivity equations, which were computed using `ode45` with relative and absolute tolerances both set to 10^{-10}; the expressions for the exact analytical sensitivity equations can be found in Kamalzare (2014).

3.4 Design of the optimal base isolation

To find the "best" choice of the design parameters, one may use a parameter study over a fine grid of design variable values or a conventional gradient-based optimization algorithm, with comparisons of some performance metric(s) to those of a baseline design. Studies in the literature have employed objectives such as minimizing the superstructure drift or absolute acceleration subject to a constraint on the base drift; others have used reliability measures. Here, a cost functional expressed in terms of mean square (MS) responses is used, defined as a weighted linear combination of the MS base drift $\sigma^2_{u_\mathrm{b}}$ and the MS absolute roof acceleration $\sigma^2_{\ddot{u}^\mathrm{a}_\mathrm{r}}$, where $\ddot{u}^\mathrm{a}_\mathrm{r} = \ddot{u}_{94} + \ddot{u}_\mathrm{g}$, as follows

$$J(\boldsymbol{\theta}) = [\sigma^2_{u_\mathrm{b}}(\boldsymbol{\theta}) / \sigma^2_{u_\mathrm{b}}(\boldsymbol{\theta}^0)] + [\sigma^2_{\ddot{u}^\mathrm{a}_\mathrm{r}}(\boldsymbol{\theta}) / \sigma^2_{\ddot{u}^\mathrm{a}_\mathrm{r}}(\boldsymbol{\theta}^0)] \tag{19}$$

where $\sigma^2_{(\cdot)}(\boldsymbol{\theta}^0)$ is a MS response of a baseline design. A MS response is approximated herein as

$$\sigma^2_{u_\mathrm{b}} = \tfrac{1}{t_\mathrm{f}} \int_0^{t_\mathrm{f}} u^2_\mathrm{b}(t)\mathrm{d}t \cong \tfrac{1}{N} \sum_{k=0}^{N} u^2_{\mathrm{b},k} \tag{20}$$

where $t_\mathrm{f} = N\Delta t$ is the simulation duration and $u_{\mathrm{b},k} = u_\mathrm{b}(k\Delta t)$. The optimization is performed using a gradient-based active-set algorithm, the `fmincon` command in MATLAB$^{\mathrm{TM}}$. The derivative of the cost functional with respect to the design parameters is given by

$$\frac{\partial J}{\partial \boldsymbol{\theta}} = \frac{2}{N} \sum_{k=0}^{N} \left[\frac{u_{\mathrm{b},k}}{\sigma^2_{u_\mathrm{b}}(\boldsymbol{\theta}^0)} \frac{\partial u_{\mathrm{b},k}}{\partial \boldsymbol{\theta}} + \frac{\ddot{u}^\mathrm{a}_{\mathrm{r},k}}{\sigma^2_{\ddot{u}^\mathrm{a}_{\mathrm{r},k}}(\boldsymbol{\theta}^0)} \frac{\partial \ddot{u}^\mathrm{a}_{\mathrm{r},k}}{\partial \boldsymbol{\theta}} \right] \tag{21}$$

`fmincon` is selected because it can exploit gradient information, which is available through Eq. (21), and can accommodate the constraints: (*i*) the yield force is always strictly positive, $Q_\mathrm{y} > 0$; (*ii*) the pre-yield stiffness is greater than or equal the post-yield stiffness, $k_\mathrm{pre} \geq k_\mathrm{post}$; and (*iii*) the post-yield stiffness is always non-negative, $k_\mathrm{post} \geq 0$.

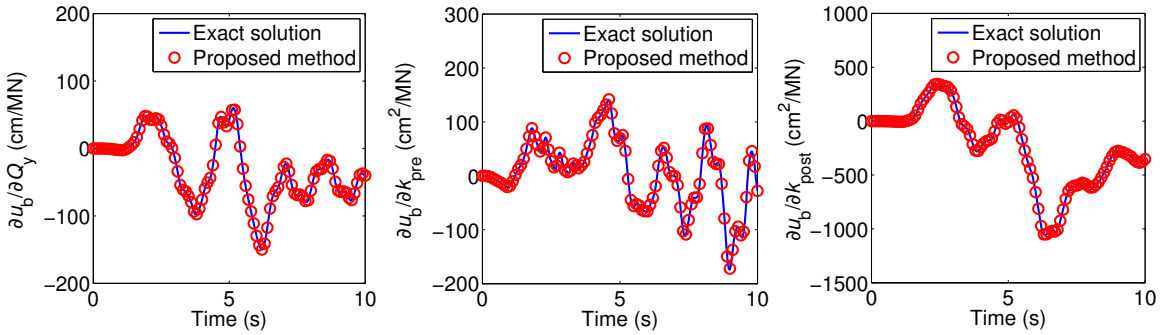

(a) Sensitivity w.r.t. Q_y (b) Sensitivity w.r.t. k_pre (c) Sensitivity w.r.t. k_post

Fig. 2 Base drift response sensitivity to the design parameters when subjected to the 1940 El Centro ground motion at the design point

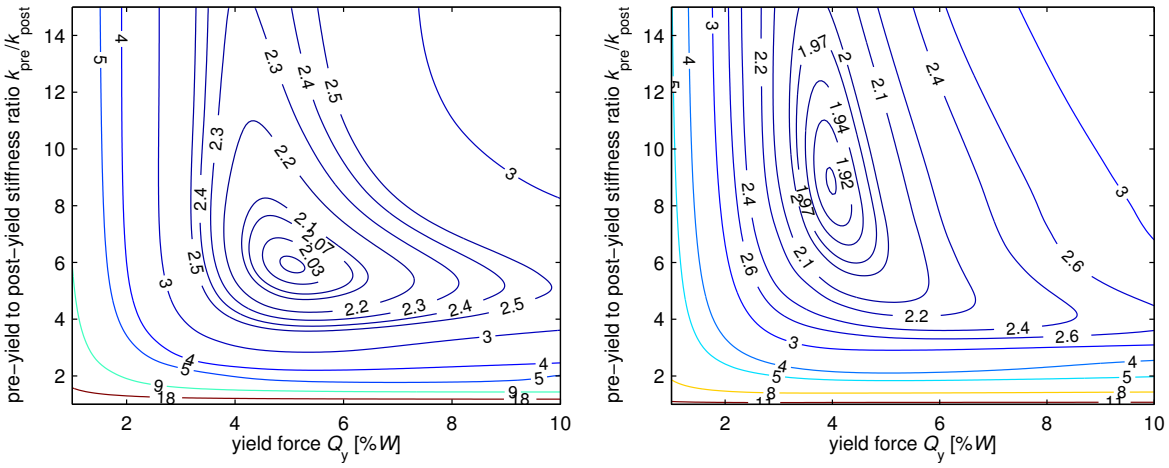

(a) 1940 El Centro (b) 1994 Northridge-Saticoy

Fig. 3 Cost contours as a function of two design parameters for two historical earthquakes

3.5 Preliminary Optimization over Q_y and k_{pre}

A preliminary study of this example in which only Q_y and k_{pre} are free design variables is useful as a first step since the response metrics can be computed over a fine grid of the two design variables to verify that the method is efficient and accurate. This simpler design optimization problem, discussed in greater detail in Johnson *et al.* (2013), uses the same model but fixes exponent $n = 1$ and post-yield stiffness $k_{post} = k_b$. Considering the cost functional Eq. (19), the design point for the El Centro earthquake is determined to be ($0.0507W$, $5.94k_b$), which results (not surprisingly) in basically the same RMS base drift and roof acceleration performances as the baseline ($0.05W$, $6k_b$). A record from the 1994 Northridge earthquake with a PGA similar to that of the El Centro record was also used for this 2-D optimization: the E-W motion of the Northridge earthquake recorded at the USC 90003 station at 17645 Saticoy St (PGA 0.368 g); using the same baseline ($0.05W$, $6k_b$), the optimization converges to a different design point ($0.0401W$, $8.73k_b$) for Northridge-Saticoy, which results in reductions of about 1% and 4% in RMS base drift and roof acceleration, respectively, relative to the baseline. To converge to the design point, these solutions required only 6 iterations, making a total of 19 function evaluations, for the El Centro earthquake, and 13 iterations (29 function evaluations) for Northridge-Saticoy; the quick convergence is facilitated by providing the gradient information. The proposed method was found to provide an optimization that is about an order of magnitude faster than with the conventional solver `ode45`. To verify that these optimizations converged to the correct results, a parameter study was performed over the two-dimensional design space as shown in Fig. 3, which confirms that the cost functionals are convex and well-behaved around the design points.

3.6 Optimization over Q_y, k_{pre} and k_{post}

The preliminary study in the previous section assumes a fixed post-yield stiffness $k_{post} = k_b$,

which likely limits the isolation performance and the optimal isolation design may be rather different if post-yield stiffness is included as a design variable. Thus, the full design space in this example includes the yield force Q_y, the pre-yield stiffness k_{pre} and the post-yield stiffness k_{post}; variations in these values are achievable in practice by changing the isolation device characteristics (*e.g.*, physical device size, proportion of lead plug to rubber/steel, ratio of steel-to-rubber, etc.). The initial guess to start the optimization is chosen to be the same as the baseline values: $(Q_y, k_{pre}, k_{post})_{initial} = (0.05W, 6k_b, k_b)$ and $(0.15W, 10k_b, k_b)$ for the El Centro and Northridge earthquakes, respectively.

The design point for the El Centro earthquake is determined to be $(0.0641W, 5.75k_b, 0.484k_b)$, which results in reductions of about 6% and 11% in RMS base drift and roof acceleration, respectively, relative to the baseline $(0.05W, 6k_b, k_b)$. When the Northridge (Sylmar) earthquake excitation is applied to the system, the optimization yields a different design point $(0.1371W, 12.45k_b, 0.61k_b)$, which results in reductions of about 4% and 8% in RMS base drift and roof acceleration, respectively, relative to the baseline $(0.15W, 10k_b, k_b)$. To converge to the design point, these solutions required only 12 iterations (26 function evaluations) for the El Centro earthquake, and 18 iterations (43 function evaluations) for Northridge; the quick convergence is again facilitated by providing the analytical gradient information from Eqs. (17) and (18).

To verify that these optimizations converged to the correct results, a small parameter study was performed. Fig. 4 shows contour line slices of the cost functional for the El Centro and Northridge (Sylmar) earthquake excitations. Clearly, each design point found by the optimization is in the region of the cost functional minimum, around which the cost functional is convex.

3.7 Timing and accuracy of the proposed approach

In this section, the computational cost of the proposed optimization method is compared with one employing a conventional nonlinear solver: the `ode45` command in MATLAB. The accuracy of both `ode45` and the proposed method can be tuned, the former by setting options for the absolute and relative tolerances, and the latter by choosing the integration time step. To ensure a fair comparison, preliminary studies showed that the accuracy of `ode45` with the default parameters (relative tolerance 10^{-3}, absolute tolerance 10^{-6}) and the proposed method using a second-order accurate trapezoidal integration with 2^{15} time steps of $\Delta t = 0.92$ ms duration each, both give relative response accuracy of order 10^{-3}. Fig. 5 shows the accuracy of the proposed method using graphs of base drift and absolute roof acceleration of the structure, respectively, at the design point for the El Centro excitation as calculated by the proposed method as well as a reference "exact" solution calculated by `ode45` with the relative and absolute tolerances both set to 10^{-10}. The computational cost of the proposed method includes one-time calculations and repeated ones that, in this example at the design point, take about 2.13 s and 5.81 s, respectively, on a computer with a 3.4 GHz Intel core i7-2600 processor and 8 GB of RAM, running MATLAB R2013a under Windows 7. The same calculation takes about 87.50 s if MATLAB's `ode45` (with default tolerances) is used as the solver. This leads to a computation speed-up of 11.0 for a single simulation but 14.8 in a typical optimization with 25 function evaluations performed.

Computing the sensitivities of the cost functional with respect to the three design parameters at each step doubles or triples the computation time, relative to computing the cost functional alone, of both MATLAB's `ode45` and the proposed method; however, as expected, including gradient information results in much faster convergence to the "optimal" design point: for El Centro,

MATLAB's `fminsearch` (a non-gradient based method) takes about 53 iterations (118 function evaluations), which is 4–5 times larger than for the gradient-based `fmincon`, so, at least for this example, there is a clear computational benefit provided by including the analytical gradients.

Note that the proposed method here uses a subdivision of the convolution space to compute portions of the integral in the Volterra integral equation using fast Fourier transforms (Gaurav *et al.* 2011); further, the accuracy and computational efficiency would be expected to be even more superior if the fourth-order integration previously discussed by the authors (Gaurav *et al.* 2011) were used instead of the second-order trapezoidal integration adopted in this study.

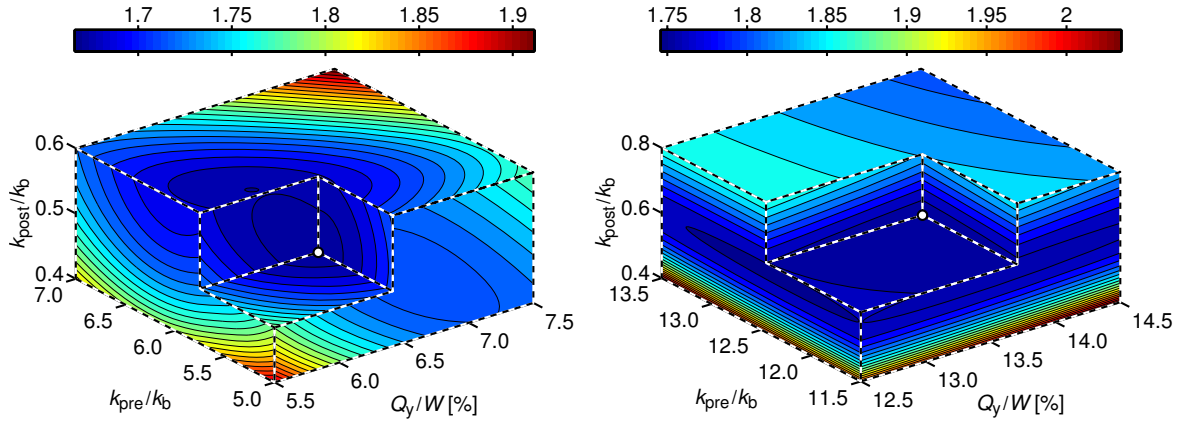

(a) 1940 El Centro earthquake (b) 1994 Northridge (Sylmar) earthquake

Fig. 4 Contour lines of the cost as a function of the design parameters for two earthquakes. The apex of the cutout shows the optimal design location

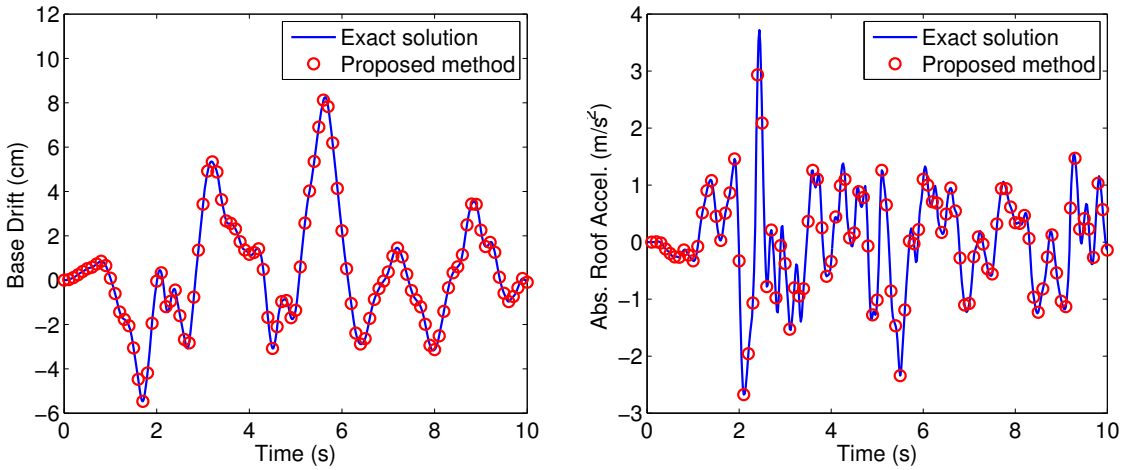

(a) Base drift response. (b) Absolute roof acceleration response.

Fig. 5 Structural responses to the El Centro earthquake using the design point isolation

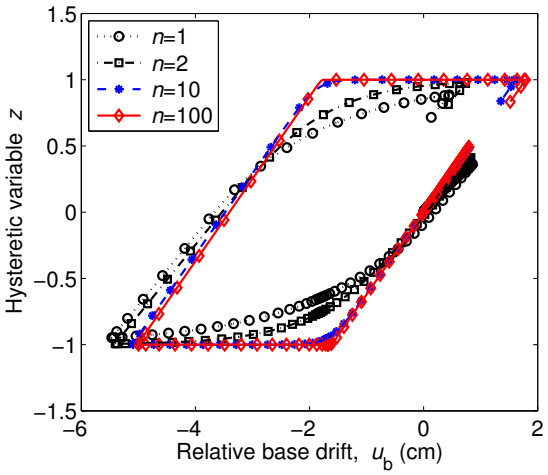

Fig. 6 Single hysteresis loop using the design point isolation calculated for different exponents n when subject to the El Centro earthquake

3.8 Investigation of the transitional region of the Bouc-Wen model

Traditionally, for the sake of simplicity, many researchers have used the bilinear behavior for the hysteretic loops. However, the Bouc-Wen model introduced in Eq. (12(a)) provides a formulation that allows modeling a smooth transition from the pre-yield to post-yield regions. This is mainly controlled by the exponent n, which is greater than or equal to 1. Using $n = 1$ results in a very smooth transition and $n \to \infty$ models the strict bilinear loops; the most common values used in the literature are $n = 1$, 2 and ∞. Among all parameters in this Bouc-Wen model (i.e., Q_y, k_{pre}, k_{post} and n), n is the one with the least tangible physical meaning; thus, this final section investigates the effect on the optimal isolator design of assuming different values for n.

As shown in Fig. 6, the shape of the hysteresis loops changes significantly for different values of n and, as expected, will result in a different "optimal" design point. Assuming the same baseline performance, the optimization is repeated for $n = 1$, 2, 10 and 100 and the design points and performance metrics (RMS base drift and roof acceleration) are shown in Table 1 for the El Centro earthquake. It is clear that the "optimal" Q_y and k_{post} are very sensitive to the value of n as they change by 21% and 130%, respectively, in this example as n changes from 1 to 100. In contrast, k_{pre} changes very slightly and appears relatively insensitive to exponent n.

It is also important to investigate the effect on response when the isolators are designed using an inaccurate value of n. (The effects of incorrect Q_y, k_{pre} and k_{post} are not studied herein because they can be experimentally determined fairly easily for a particular device whereas the exponent n is often neglected in curve-fitting from laboratory tests.) The response metrics for the system at the design points shown in Table 1 are evaluated for isolators with different n values and the percentage change in their performance metrics, compared to the original design point responses, are calculated and shown in Table 2. It is reported in the literature (Skinner *et al.* 1993, Nagarajaiah and Sun 2000) that assuming bilinear hysteresis overestimates the roof acceleration; this is confirmed by comparing the corresponding columns of Table 2. This study shows that

designing with a larger n always results in overestimating the actual RMS roof acceleration; but, no clear conclusions can be made about the RMS base drift. Further investigations (not included here for the sake of brevity) showed that the peak base drift and peak roof acceleration have similar variation trends as the corresponding RMS metrics, though the changes are less significant and mostly remain less than 4–5%.

4. Conclusions

To enable the optimal design of passive isolation systems, this paper proposes extending a computationally efficient approach previously developed by the authors for systems with local features (linear or nonlinear, deterministic or random) but are otherwise linear. This approach can provide highly efficient simulation of both responses and their sensitivities to the design parameters in the isolation element models. The methodology was briefly summarized and then applied to the optimal design of a base isolation system to find the optimal yield force and pre-yield and post-yield stiffnesses of a hysteretic isolation layer for an 11-story 2-bay isolated building. The isolator was modeled with Bouc-Wen hysteresis and (small) viscous damping. A baseline design, using a yield force that is 5% or 15% of the building weight and a pre-yield stiffness that is 6 or 10 times that of the post-yield stiffness, as suggested in the literature for a moderate and strong ground motions, respectively, are used for comparison. The optimal design for the El Centro earthquake results in about 6% and 11% reductions in RMS base drift and roof acceleration, respectively, relative to the baseline; for the Northridge earthquake, the corresponding reductions are 4% and 8%, respectively.

Table 1 Design points for different exponent n values for the El Centro earthquake

n	1	2	10	100
Q_y/W [%]	6.4142	5.8800	5.0892	5.0613
k_{pre}/k_b	5.7506	5.3100	5.3099	5.3527
k_{post}/k_b	0.4840	0.5490	1.0508	1.1144
σ_{u_b} [% change rel. to $\sigma^0_{u_b}$]	–6.42	–2.54	3.20	2.96
$\sigma_{\ddot{u}^a_r}$ [% change rel. to $\sigma^0_{\ddot{u}^a_r}$]	–10.81	–10.20	–6.44	–4.82
J	1.67	1.76	1.94	1.97

Table 2 RMS base drift and roof acceleration percent changes when the design points are evaluated at different exponent n values

	RMS base drift changes (%)				RMS roof acceleration changes (%)			
	Actual exponent n				Actual exponent n			
Design n	1	2	10	100	1	2	10	100
1	0	–1.57	8.27	10.93	0	9.98	20.62	22.31
2	3.51	0	6.24	9.25	–8.18	0	8.51	9.64
10	3.66	–0.72	0	0.58	–11.19	–5.87	0	0.86
100	3.94	–0.73	–0.47	0	–11.56	–6.48	–0.80	0

The proposed approach was able to perform the design optimization function evaluation simulations more than one order of magnitude faster; the computation speed-up was 14.8 for a typical parameter study or iterative optimization of this relatively small numerical example. However, since various types of passive structural control elements are being studied for large structures, such as high-rise buildings and long-span bridges, requiring far more complex models than the numerical considered herein, the gains in computational efficiency of the proposed optimization method are expected to be even more pronounced for such structural models.

Acknowledgments

The authors gratefully acknowledge support of this work by the National Science Foundation through awards CMMI 11-00528, 11-33023, and 13-44937. Any opinions, findings, and conclusions or recommendations expressed herein are those of the authors and do not necessarily reflect the views of the National Science Foundation. The first author also acknowledges the support of a Viterbi Doctoral Fellowship from the University of Southern California.

References

Bhatti, M.A., Pister, K.S. and Polak, E.L. (1978), *Optimal design of an earthquake isolation system*, Report No. UCB/EERC-78/22, Earthquake Engineering Research Center, University of California, Berkeley.

Bouc, R. (1967), "Forced vibration of mechanical systems with hysteresis", *Proceedings of the 4th Conference on Nonlinear Oscillation*, Prague, Czechoslovakia, 315.

Bucher, C. (2009), "Probability-based optimal design of friction-based seismic isolation devices", *Struct. Saf.*, **31**(6), 500-507.

Buckle, I.G. and Mayes, R.L. (1990), "Seismic isolation: History, application, and performance—a world view", *Earthq. Spectra*, **6**(2), 161-201.

Constantinou, M.C. and Tadjbakhsh, I.G. (1983), "Probabilistic optimum base isolation of structures", *J. Struct. Eng. - ASCE*, **109**(3), 676-689.

Constantinou, M.C. and Tadjbakhsh, I.G. (1984), "The optimum design of a base isolation system with frictional elements", *Earthq. Eng. Struct. D.*, **12**(2), 203-214.

Constantinou, M.C. and Tadjbakhsh, I.G. (1985), "Hysteretic dampers in base isolation: Random approach", *J. Struct. Eng. - ASCE*, **111**(4), 705-721.

Fragiacomo, M., Rajgelj, S. and Cimadom, F. (2003), "Design of bilinear hysteretic isolation systems", *Earthq. Eng. Struct. D.*, **32**(9), 1333-1352.

Gaurav, Wojtkiewicz, S.F. and Johnson, E.A. (2011), "Efficient uncertainty quantification of dynamical systems with local nonlinearities and uncertainties", *Probabilist. Eng. Mech.*, **26**(4), 561-569.

Gordis, J.H. and Radwick, J. (1999), "Efficient transient analysis for large locally nonlinear structures", *Shock Vib.*, **6**(1), 1-9.

Housner, G.W., Bergman, L.A., Caughey, T.K., Chassiakos, A.G., Claus, R.O., Masri, S.F., Skelton, R.E., Soong, T.T., Spencer, B.F. and Yao, J.T.P. (1997), "Structural control: Past, present, and future", *J. Eng. Mech. - ASCE*, **123**(9), 897-971.

Jangid, R. (2000), "Optimum frictional elements in sliding isolation systems", *Comput. Struct.*, **76**(5), 651-661.

Jangid, R. (2005), "Optimum friction pendulum system for near-fault motions", *Eng. Struct.*, **27**(3), 349-359.

Jangid, R. (2007), "Optimum lead-rubber isolation bearings for near-fault motions", *Eng. Struct.*, **29**(10), 2503-2513.

Jensen, H. and Sepulveda, J. (2012), "On the reliability-based design of structures including passive energy

dissipation systems", *Struct. Saf.*, **34**(1), 390-400.
Johnson, E.A., Kamalzare, M. and Wojtkiewicz, S.F. (2013), "Efficient optimal design of passive hysteretic base isolators by Volterra integral equations", *Proceedings of the 11th International Conference on Structural Safety & Reliability (ICOSSAR 2013)*, New York, NY, June 16-20.
Johnson, E.A. and Wojtkiewicz, S.F. (2014), "Efficient sensitivity analysis of structures with local modifications — Part II: Transfer functions and spectral densities", *J. Eng. Mech. - ASCE*, **140**(9), 04014068.
Kamalzare, M. (2014), *Computationally efficient design of optimal strategies for passive and semiactive damping devices in smart structures*, Ph.D. Dissertation, Univ. of Southern California, Los Angeles, CA.
Kamalzare, M., Johnson, E.A. and Wojtkiewicz, S.F. (2015), "Computationally efficient design of optimal strategies for controllable damping devices", *Struct. Control Health Monit.*, **22**(1), 1-18.
Kelly, J.M. (1986), "Aseismic base isolation: review and bibliography", *Soil Dyn. Earthq. Eng.*, **5**, 202-216.
Naeim, F. and Kelly, J.M. (1999), *Design of Seismic Isolated Structures: From Theory to Practice*, Wiley, Chichester, England.
Nagarajaiah, S. and Sun, X. (2000), "Response of base-isolated USC hospital building in Northridge earthquake", *J. Struct. Eng. - ASCE*, **126**(10), 1177-1186.
Norton, K.M. (2002), *Parameter optimization of seismic isolator models using recursive block-by-block nonlinear transient structural synthesis*, M.S. thesis, Naval Postgraduate School, Monterey, CA.
Park, J.G. and Otsuka, H. (1999), "Optimal yield level of bilinear seismic isolation devices", *Earthq. Eng. Struct. D.*, **28**(9), 941-955.
Roy, B.K., Chakraborty, S. and Mihsra, S.K. (2014), "Robust optimum design of base isolation system in seismic vibration control of structures under uncertain bounded system parameters", *J. Vib. Control*, **20**(5), 786-800.
Skinner, R.I., Robinson, W.H. and McVerry, G.H. (1993), *An Introduction to Seismic Isolation*, Wiley, Chichester, England.
Soong, T.T. and Dargush, G.F. (1997), *Passive Energy Dissipation Systems in Structural Engineering*. Wiley, Chichester, England.
Taflanidis, A.A. and Beck, J.L. (2008a), "An efficient framework for optimal robust stochastic system design using stochastic simulation", *Comput. Method. Appl. M.*, **198**(1), 88-101.
Taflanidis, A.A. and Beck, J.L. (2008b), "Stochastic subset optimization for optimal reliability problems", *Probabilist. Eng. Mech.*, **23**(2-3), 324-338.
Taflanidis, A.A. and Beck, J.L. (2009), "Stochastic subset optimization for reliability optimization and sensitivity analysis in system design", *Comput. Struct.*, **87**(5-6), 318-331.
Taflanidis, A.A. and Beck, J.L. (2010), "Reliability-based design using two-stage stochastic optimization with a treatment of model prediction errors", *J. Eng. Mech. - ASCE*, **136**(12), 1460-1473.
Wen, Y.K. (1976), "Method for random vibration of hysteretic systems", *J. Eng. Mech. Div.*, **102**(2), 259-263.
Wilson, E.L. (1999), *Three Dimensional Static and Dynamic Analysis of Structures: A Physical Approach with Emphasis on Earthquake Engineering*, Computers and Structures, 3rd Ed.
Wojtkiewicz, S.F. and Johnson, E.A. (2014), "Efficient sensitivity analysis of structures with local modifications — Part I: Time domain responses", *J. Eng. Mech. - ASCE*, **140**(9), 04014067.